Available online at www.sciencedirect.com
ScienceDirect
Journal of Solid State Chemistry 180 (2007) 410–419
JOURNAL OF SOLID STATE CHEMISTRY
www.elsevier.com/locate/jssc

# Crystal structure and phonon properties of noncentrosymmetric $LiNaB_4O_7$

M. Mączka[a,*], A. Waśkowska[a], A. Majchrowski[b], J. Żmija[b], J. Hanuza[a,c], G.A. Peterson[d], D.A. Keszler[d]

[a]Institute of Low Temperature and Structure Research, Polish Academy of Sciences, P.O. Box 1410, 50-950 Wrocław 2, Poland
[b]Institute of Applied Physics, Military University of Technology, 2 Kaliskiego Street, 00-908 Warszawa, Poland
[c]Department of Bioorganic Chemistry, Faculty of Industry and Economics, University of Economics, ul. Komandorska 118/120, 53-345 Wrocław, Poland
[d]Department of Chemistry, 153 Gilbert Hall, Oregon State University, Corvallis, OR 97331-4003, USA

Received 9 June 2006; received in revised form 20 October 2006; accepted 21 October 2006
Available online 9 November 2006

**Abstract**

A new borate, $LiNaB_4O_7$, has been synthesized and characterized by single-crystal X-ray structure determination. The material crystallizes in the orthorhombic system, noncentrosymmetric space group *Fdd*2, with unit cell dimensions $a = 13.325(2)$, $b = 14.099(2)$, $c = 10.243(2)$ Å, $Z = 16$, and $V = 1924.3(7)$ Å$^3$. Like $Li_2B_4O_7$, the structure is built of two symmetrically independent, interpenetrating $(B_4O_7)^3_\infty$ polyanionic frameworks built from condensation of the $B_4O_9$ fundamental building block, which is comprised of two distorted $BO_4$ tetrahedra and two $BO_3$ triangles. The interpenetrating frameworks produce distinct tunnels that are selectively occupied by the Li and Na atoms. Large single crystals exhibiting an optical absorption edge with $\lambda < 180$ nm have been grown via the top-seeded-solution-growth method. The SHG signal (0.15 × potassium dihydrogen phosphate (KDP)) is consistent with the calculated components of the SHG tensor and the approximate centrosymmetric disposition of the independent and interpenetrating $(B_4O_7)^3_\infty$ frameworks. A complete analysis of polarized IR and Raman spectra confirms a close relationship between the title compound and $Li_2B_4O_7$.


*Keywords:* $LiNaB_4O_7$ borate; Crystal structure; Phonon properties; Second-harmonic generation

## 1. Introduction

Borates play an important role among known nonlinear optical materials, since many such crystals exhibit useful high $\chi^{(2)}$- and $\chi^{(3)}$-nonlinear susceptibilities [1], short cut-off wavelengths extending into the deep UV, and an outstanding resistance to laser damage [1–4]. Czochralski and Bridgman-grown crystals of $Li_2B_4O_7$ (LTB) are representative of these borates, exhibiting transparency from 170 to 3300 nm and capabilities for fourth- and fifth-harmonic generation of 1064-nm laser radiation [5]. LTB crystals have also been extensively studied for use in surface acoustic wave devices [6–8] and thermoluminescence dosimeters [9].

The crystal structure of LTB has been reported to belong to the tetragonal space group $I4_1cd$ ($C_{4v}{}^{12}$) with the unit cell parameters $a = 9.477$ Å, $c = 10.286$ Å, and $Z = 8$ [10,11]. The structure contains a $B_4O_9$ fundamental building block (Fig. 1) of two $BO_4$ vertex-sharing tetrahedra and two bridging $BO_3$ triangles. These groups condense through the nonbridging O atoms to produce the $(B_4O_5O_{4/2})^3_\infty = (B_4O_7)^3_\infty$ framework.

Raman and IR spectroscopic studies have been reported for LTB crystals in several papers [12–17]. These data were used to confirm the symmetry and to propose assignments of the observed modes to the respective motions of atoms. The performed studies showed that most of the $A_1$ modes revealed the weak polar character and, therefore, only five $A_1$ modes at 156, 255, 341, 687, and 778 cm$^{-1}$ displayed a significant LO–TO splitting.

Here we report the results of synthesis, X-ray diffraction, optical transmission, SHG, Raman, and IR studies on

*Corresponding author. Fax: +48 71 344 1029.
*E-mail address:* m.maczka@int.pan.wroc.pl (M. Mączka).

0022-4596/$ - see front matter © 2006 Elsevier Inc. All rights reserved.
doi:10.1016/j.jssc.2006.10.035

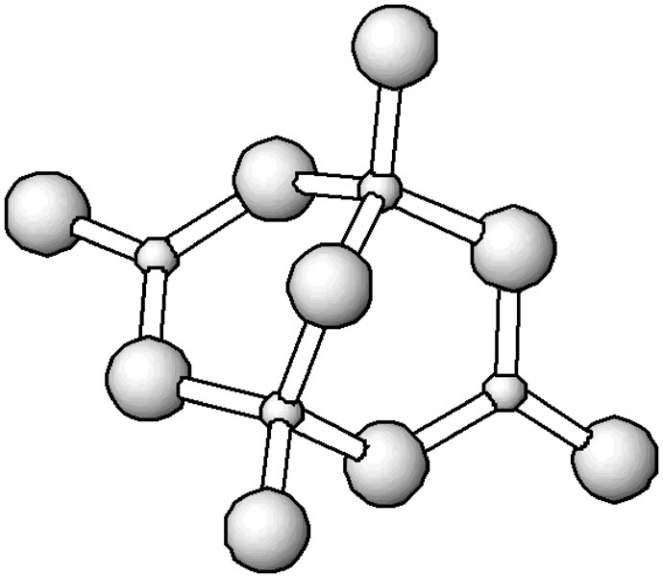

Fig. 1. Fundamental building block, $B_4O_9$, for the polyborate framework in $Li_2B_4O_7$ and $LiNaB_4O_7$.

$LiNaB_4O_7$, a new compound that has been identified during our attempts to synthesize new nonlinear optical materials. We demonstrate that $LiNaB_4O_7$ exhibits a noncentrosymmetric structure similar to that of $Li_2B_4O_7$, but partial substitution of Na for Li leads to a reduction in crystal symmetry and significant changes in the phonon properties.

## 2. Experimental section

The phase diagram for the binary system $Li_2B_4O_7$–$Na_2B_4O_7$ was examined by using differential thermal analysis (DTA). Selected compositions of the end members were placed in covered platinum crucibles on a TA Instruments, Model 2920 Modulated DSC with a 1873-K DTA module. A flow of $N_2$(g) at 30 mL/min was used, and a heating rate of 5 °C/min was employed after the furnace was stabilized at 550 °C.

LNTB single crystals were grown by the top-seeded-solution-growth (TSSG) method from a solution containing 65 mol% $Na_2B_4O_7$ and 35 mol% $Li_2B_4O_7$. A detailed description of our TSSG apparatus and methodology can be found elsewhere [18]. Experiments were carried out with a two-zone resistance-heated furnace and a platinum crucible 40 mm in height and diameter. To achieve supersaturation, leading to crystallization of LNTB at approximately 730 °C, the melt temperature was lowered at a rate of 0.05 °C/h. The growing LNTB crystals were rotated at a rate of 5 rpm and very slowly pulled at a rate of 1 mm/day.

The chemical compositions of the crystals were analyzed by using X-ray fluorescence with an EDAX 9800 microanalyzer. Although the light elements Li and B cannot be satisfactorily determined by EDAX measurement, the O/Na ratio could be established.

A small crystal was isolated from the boule and used for intensity data collection with an Oxford Diffraction/CCD single-crystal X-ray diffractometer, operating in the $\kappa$ geometry with graphite monochromated Mo$K\alpha$ radiation. The intensity data were collected with the $\omega$-scan technique, steps of $\Delta\omega = 1.0^\circ$, and an exposure time of 25 s/image. Crystal and instrumental stability were monitored by measuring a standard image after each set of 50 images [19]; no significant changes in diffracted intensities were observed during the course of data collection. The intensities, corrected for Lorentz-polarization effects, were integrated and a numerical absorption correction based on the crystal shape was applied [20]. The structure was solved with direct methods by using the SHELXS97 program [21] and subsequent difference Fourier calculations. The structure refinement calculations were performed with the SHELXL97 package [22]. Site occupancy factors were refined for the Li and Na sites; the refined parameters differed from full occupancy by less than $2\sigma$, so they were subsequently fixed at unity. Because of the small values of the anomalous dispersion corrections $\Delta f''$, assignment of the absolute configuration on the basis of the Flack parameter was not conclusive. Crystal data, experimental details, and refinement parameters are summarized in Table 1. Atomic positions and equivalent isotropic displacement parameters are listed in Table 2. Complete structural data have been deposited with Fachinformationszentrum (FIZ) Karlsruhe, Informationsdienste ICSD, D-76344 Eggenstein-Leopoldshafen, Germany (e-mail: crysdata@fiz-karlsruhe.de) under the CSD number 416956 (filename LiNaB4O7.cif).

The optical transmittance spectrum was recorded at room temperature by using a 1.24-mm thick slab of LNTB polished on both sides and a Cary 5E spectrophotometer with a range of 180–3300 nm. The method of Kurtz and Perry [23] was used to measure the second-harmonic signal of a powder of the title compound relative to that of a sample of potassium dihydrogen phosphate (KDP). The samples were pressed between glass microscope cover slides and secured with tape in 1-mm thick aluminum holders containing a 5-mm diameter hole. The holders were placed in a light-tight box and excited with 20-mJ pulses from a Q-switched Nd:YAG laser (New Wave Research Minilase-20, $\lambda = 1064$ nm). The incident beam was passed through a long-pass filter to eliminate flash-lamp light and then directed onto the samples. The second-harmonic signal was collected through an interference filter ($530 \pm 10$ nm) with a photomultiplier attached to a Tektronix SC504 80-MHz oscilloscope. A null reading was established by measuring the signal for the centrosymmetric material $Al_2O_3$. SHG coefficients, $d_{jm}$, were calculated on the basis of a symbolic addition method [24].

Polycrystalline infrared spectra were measured with a Biorad 575C FT-IR spectrometer as KBr pellets in the 1500–400 $cm^{-1}$ region and in Nujol suspension for the 500–30 $cm^{-1}$ region. Polarized spectra of a single crystal were measured with a Biorad 575C FT-IR spectrometer by

using a fixed-angle specular reflectance accessory. Raman spectra were measured in back-scattering geometry with a Bruker FT-Raman RFS 100/S spectrometer and 1064-nm excitation. The IR and Raman spectra were recorded with a spectral resolution of $2\,cm^{-1}$.

Table 1
Crystal data, experimental details and structure refinement results for LNTB

| | |
|---|---|
| *Crystal data* | |
| Crystal system, space group | Orthorhombic, *Fdd*2 |
| Unit cell dimensions (Å) | |
| *a* | 13.325(3) |
| *b* | 14.099(3) |
| *c* | 10.7243(2) |
| Volume (Å$^3$) | 1924.3(7) |
| *Z*, Calculated density (mg/m$^3$) | 16, 2.557 |
| Crystal size (mm) | $0.27 \times 0.27 \times 0.29$ |
| *Data collection* | |
| Wavelength (Å) | 0.71073 |
| Temperature (K) | 297 |
| $2\theta$ max for data collection | 87.56 |
| Limiting indices | |
| *h* | −15, 26 |
| *k* | −19, 28 |
| *l* | −20, 14 |
| Reflections collected | 9941 |
| Reflections unique | 3265 |
| Reflections $>2\sigma(I)$] | 2430 |
| Absorption coefficient (mm$^{-1}$) | 0.310 |
| Absorption correction | Numerical |
| *r*(int) before, after abs. correction | 0.0318, 0.0285 |
| *Refinement* | |
| Refinement method | Full-matrix least-squares on $F^2$ |
| Number of refined parameters | 120 |
| Goodness-of-fit on $F^2$ | 1.010 |
| Final *R* indices [$I>2\sigma(I)$] | |
| $R_1$ | 0.0438 |
| $wR_2$ | 0.0944 |
| Extinction coefficient | 0.0003 (3) |
| Largest diff. peak and hole (e/Å$^3$) | 0.50 and −0.61 |

Table 2
Fractional atomic coordinates ($\times 10^4$) and equivalent isotropic displacement parameters (Å$^2 \times 10^3$) for LNTB

| | *x* | *y* | *z* | *U* (eq) |
|---|---|---|---|---|
| O (1) | 726 (1) | 2017 (1) | 100 (1) | 14 (1) |
| O (2) | 2500 | 2500 | −26 (1) | 13 (1) |
| O (3) | 1954 (1) | 1410 (1) | 1643 (1) | 15 (1) |
| O (4) | 1351 (1) | 3034 (1) | 1676 (1) | 14 (1) |
| B (1) | 1645 (1) | 2230 (1) | 803 (1) | 11 (1) |
| B (2) | 449 (1) | 1215 (1) | −523 (2) | 11 (1) |
| O (5) | 2053 (1) | 827 (1) | 5286 (1) | 12 (1) |
| O (6) | 2500 | 2500 | 5143 (1) | 10 (1) |
| O (7) | 2900 (1) | 1526 (1) | 7021 (1) | 12 (1) |
| O (8) | 1198 (1) | 2039 (1) | 6641 (1) | 12 (1) |
| B (3) | 2154 (1) | 1728 (1) | 5974 (1) | 9 (1) |
| B (4) | 1261 (1) | 442 (1) | 4656 (1) | 9 (1) |
| Na | 1012 (1) | 2391 (1) | 3750 (1) | 26 (1) |
| Li | 45 (2) | 3597 (3) | 1243 (4) | 41 (1) |

$U_{eq} = 1/3\Sigma_i\Sigma_j U_{ij} a_i^* a_j^* \mathbf{a}_i \mathbf{a}_j$.

## 3. Results and discussion

### 3.1. Crystal growth and structure determination

According to the phase diagram for the binary system $Li_2B_4O_7$–$Na_2B_4O_7$ [25], Fig. 2, $LiNaB_4O_7$ (LNTB) melts incongruently at 765 °C. As such, crystals were grown from a melt rich in $Na_2B_4O_7$. The LNTB crystals exhibited strong anisotropy of growth velocities that resulted in a nonuniform growth similar to that observed during growth of polar $BiB_3O_6$ single crystals [26]. In some directions the growth was not observed at all, so the LNTB crystallization was strongly asymmetric around the seed rotation axis. Following growth for 10 days, the best LNTB crystal boule measured $1.0 \times 1.5 \times 1.5\,cm^3$. From an EDAX measurement, the O/Na ratio of the single crystals was found to be 7.19. This result is within experimental error of the formula LiNaB4O7; as noted in Section 2, the formula is also supported by the structure determination. During examination of the phase diagram, we did not observe appreciable solid solubility between LNTB and $Na_2B_4O_7$; moreover, the structure of LTNB differs markedly from $Na_2B_4O_7$, which is built from $B_5O_{11}$ groups and $B_3O_7$ rings. As determined from the phase-diagram analysis, there is nearly complete solid solubility between LTNB and LTB ($Li_{2-x}Na_xB_4O_7$, $0<x<1$). For $x<0.55$, the tetragonal LTB structure is adopted, and for $x>0.55$, the orthorhombic LNTB structure forms. Because the LNTB crystal was grown from a melt compositionally rich in $Na_2B_4O_7$, it will be saturated in Na, producing a crystal with a ratio Li:Na of 1:1.

The crystal structure of LNTB can be regarded as an orthorhombic distortion of tetragonal LTB [10,11], i.e., the orthorhombic space group *Fdd*2 of LNTB is a noniso-morphic subgroup of the tetragonal space group $I4_1cd$ of LTB. Substitution of the larger $Na^+$ ion for half of the $Li^+$ ions in LTB increases the molar volume from 115.0 to

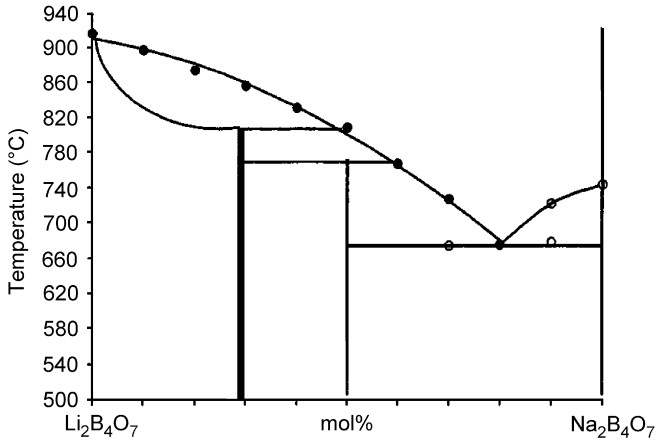


Fig. 2. Phase diagram for the system $Li_2B_4O_7$–$Na_2B_4O_7$.

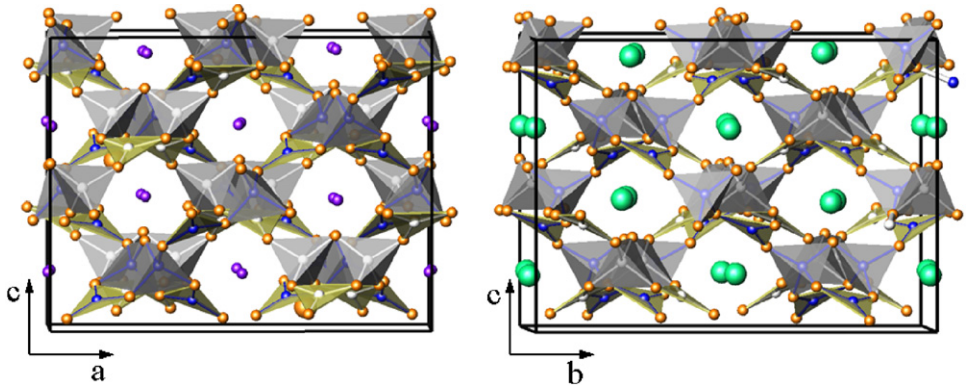


Fig. 3. Left—view of interpenetrating $B_4O_7$ frameworks in $LiNaB_4O_7$ along [010] with channels occupied by Li. Right—view of interpenetrating $B_4O_7$ frameworks in $LiNaB_4O_7$ along [100] with channels occupied by Na.

127.3 $Å^3$. In each structure, independent and interpenetrating three-dimensional polyborate frameworks are built from condensation of the building block $B_4O_9$ (Fig. 1). In LNTB, one of these frameworks contains only atoms B1, B2, O1, O2, O3, and O4, while the remaining B and O atoms comprise the other. As noted in Fig. 3, the interpenetration of the frameworks leads to unique channels extending along the *a* and *b* axes that are selectively occupied by Na and Li atoms, respectively.

Interatomic distances and angles are summarized in Table 3. Atoms B(2) and B(4) lie in planes of three O atoms. They form one short and two longer bonds; the B–O distances range from 1.350(2) to 1.379(2) Å, and the bond angles in the triangles vary between 118.6(1)° and 121.5(1)° (Table 3). The tetrahedral $BO_4$ groups centered by atoms B(1) and B(3) are strongly distorted, having two shorter and two longer B–O bonds, but the mean B–O = 1.479(1) Å distance compares well with the corresponding mean bond lengths in $LiB_3O_5$ [27], $Na_2B_4O_7$ [28], and $K_2B_4O_7$ [29]. The O–B–O angles in the tetrahedra range from 103.42(9)° to 114.88(11)°.

The Na atoms are irregularly coordinated by seven O atoms with Na–O distances ranging from 2.265(1) to 2.854(1)− Å. The broad distribution of the Na–O lengths is a common feature of the irregular coordination polyhedra about Na in complex borate framework structures [11,27–30]. Bond valence sums $\Sigma s = 1.267$ indicate that the Na atom is slightly overbonded in the material; for the B and Li atoms, the maximum deviations from the expected valence do not exceed 0.026 [31,32]. The Li atoms are (3 + 2) coordinated by O atoms forming highly distorted trigonal bipyramids. In each pyramid, three bond lengths are near 1.96 Å, defining the triangular plane, while the remaining two along the axial directions are much longer, cf., Table 3. It should be noted that the Na atoms are bound to three independent O atoms (O1, O3, and O4) from one of the $B_4O_7$ frameworks and only two atoms (O5 and O6) in the other. In a similar manner, two of the short Li–O interactions (O7 and O8) are associated with one of the frameworks, and only one (O4) involves connection to the other. These dissimilar Li–O and Na–O connections provide the basis for the chemical and crystallographic distinction of the two interpenetrating $B_4O_7$ frameworks.

The polyhedral borate framework in LNTB differs considerably from that in the homologous pair $LiKB_4O_7$ and $LiRbB_4O_7$ [30], where the larger K and Rb atoms contribute to the formation of unique structures. These compounds crystallize in the noncentrosymmetric space group $P2_12_12_1$ with the Rb derivative having a larger unit cell, $V = 1248.1(3)$ $Å^3$, than the K derivative, $V = 1197.8(3)$ $Å^3$. The $(B_3O_8)^{-7}$ anion is a six-membered ring consisting of one $(BO_3)^{3-}$ and two $(BO_4)^{5-}$ units. The $(B_3O_8)^{-7}$ rings joined by bridging O atoms form infinite spiral chains parallel to the [100] direction. The $(B_5O_{10})^{5-}$ group comprises one tetrahedrally coordinated B atom and four $BO_3$ groups, which form two six-membered rings joined via a central $BO_4$ group. In the structure the two anionic groups $(B_3O_8)^{-7}$ and $(B_5O_{10})^{5-}$ are interconnected by sharing O atoms.

### 3.2. Optical transmission and SHG

As shown in Fig. 4, the LNTB crystals exhibit high transparency in the UV region, opening a wide window for UV applications. The transmission cut-off extends to at least 180 nm, the measurement limit of the spectrophotometer. In general, the transmittance spectrum of LNTB is very similar to the transmittance spectrum of LTB crystals, which exhibit a short wavelength cut-off at 160 nm [33]. In our measurement, however, a clear, broad transmittance peak is observed near 192 nm (see inset in Fig. 4).

SHG coefficients, $d_{ijk}$, were determined by the symbolic addition of the hyperpolarizability coefficients for the individual $BO_3$ and $BO_4$ groups in the frameworks according to Eq. (1)

$$d_{ijk} = \frac{1}{V}\sum_{1}^{N}\sum_{lmn} R_{il}R_{jm}R_{kn}\beta_{lmn}, \quad (1)$$

where the components of the hyperpolarizability tensor ($\beta_{lmn}$) are summed according to the direction cosines ($R$), i.e., orientations, of the individual groups ($N$) and weighted

Table 3
Selected bond lengths (Å) and bond angles (°) for LNBO

| | |
|---|---|
| B (1)–O (1) | 1.4519 (15) |
| B (1)–O (2) | 1.4706 (16) |
| B (1)–O (4) | 1.4969 (15) |
| B (1)–O (3) | 1.4986 (15) |
| B (2)–O (1) | 1.3502 (16) |
| B (2)–O (4)#1 | 1.3730 (16) |
| B (2)–O(3)#2 | 1.3804 (16) |
| B (3)–O (6) | 1.4566 (14) |
| B (3)–O (5) | 1.4579 (14) |
| B (3)–O (7) | 1.4904 (15) |
| B (3)–O (8) | 1.5104 (15) |
| B (4)–O (5) | 1.3515 (16) |
| B (4)–O (7)#2 | 1.3772 (15) |
| B (4)–O (8)#1 | 1.3789 (14) |
| Na (1)–O (3)#3 | 2.2654 (11) |
| Na (1)–O (7)#2 | 2.2975 (11) |
| Na (1)–O (4) | 2.3533 (12) |
| Na (1)–O (5)#2 | 2.4041 (11) |
| Na (1)–O (6) | 2.4483 (10) |
| Na (1)–O (1)#4 | 2.8231 (12) |
| Na (1)–O (3) | 2.8544 (13) |
| Li (1)–O (8)#5 | 1.927 (3) |
| Li (1)–O (7)#6 | 1.957 (3) |
| Li (1)–O (4) | 1.964 (3) |
| Li (1)–O (2)#7 | 2.346 (5) |
| Li (1)–O (1) | 2.675 (5) |
| O (1)–B (1)–O (2) | 114.88 (11) |
| O (1)–B (1)–O (3) | 110.90 (10) |
| O (1)–B (1)–O (4) | 103.42 (09) |
| O (2)–B (1)–O (3) | 108.60 (09) |
| O (2)–B (1)–O (4) | 110.57 (09) |
| O (3)–B (1)–O (4) | 108.22 (10) |
| O (1)–B (2)–O (3)#2 | 119.13 (11) |
| O (1)–B (2)–O (1)#1 | 120.37 (11) |
| O (3)#2–B (2)–O (4)#1 | 120.50 (11) |
| O (5)–B (3)–O (6) | 113.46 (10) |
| O (5)–B (3)–O (7) | 104.04 (09) |
| O (5)–B (3)–O (8) | 113.19 (09) |
| O (6)–B (3)–O (7) | 110.59 (09) |
| O (6)–B (3)–O (8) | 108.33 (09) |
| O (7)–B (3)–O (8) | 107.01 (09) |
| O (5)–B (4)–O (7)#2 | 118.62 (10) |
| O (5)–B (4)–O (8)#1 | 121.51 (10) |
| O (7)#2–B (4)–O (8)#1 | 119.87 (11) |

#1: $-x+1/4$, $y-1/4$, $z-1/4$; #2: $x-1/4$, $-y+1/4$, $z-1/4$; #3: $-x+1/4$, $y+1/4$, $z+1/4$; #4: $-x$, $-y+1/2$, $z+1/2$; #5: $-x$, $y+1/2$, $z-1/2$; #6: $-x+1/4$, $y+1/4$, $z-3/4$; #7: $x-1/4$, $-y+3/4$, $z+1/4$.

by their number densities ($1/V$). In this approach, the $BO_3$ and $BO_4$ groups are treated as idealized $D_{3h}$ and $T_d$ geometries, respectively, since their relative orientations dominate the contributions to the $d_{ijk}$ coefficients. The hyperpolarizability parameters $\beta_{111}(BO_3) = \beta_{123}(BO_4)$ and number densities are scaled relative to the value of $d_{11} = 1.48$ pm/V and structural information for $YAl_3(BO_3)_4$ [34].

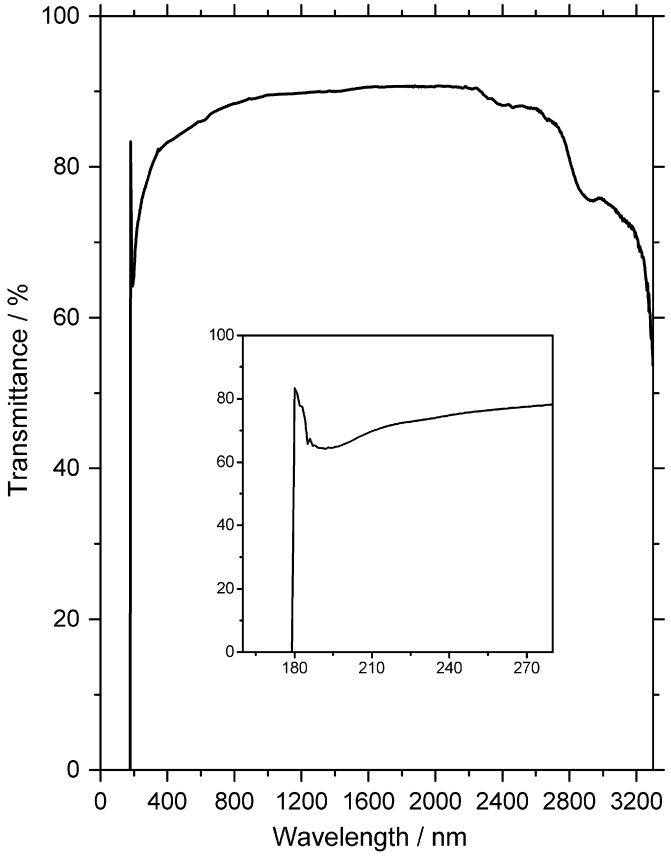


Fig. 4. Transmission spectrum of the 1.24 mm thick LNTB crystal.

For crystal class *mm*2, the coefficients in the SHG tensor and computed values for LNTB are $d_{15} = 0.08$, $d_{24} = 0.2$, $d_{31} = -0.2$, $d_{32} = 0.1$, and $d_{33} = 0.08$ pm/V. The results are in general agreement with the SHG signal of $0.15\times$ KDP ($d_{36} = 0.4$ pm/V) and the reported value of $d_{31} = 0.12$ pm/V for LTB [35]. The relatively small $d$ coefficients are consistent with the disposition of the $BO_3$ triangles and $BO_4$ tetrahedra in the structure. The independent $B_4O_7$ frameworks can be brought into approximate coincidence by translating one of them by 1/4, 1/4, 1/4 and rotating by 90° about the *c*-axis. The 90° rotation is representative of an approximate center of symmetry relating the two frameworks, which leads to a strong cancellation of the hyperpolarizability coefficients for both the $BO_3$ and $BO_4$ groups and the small bulk SHG coefficients.

### 3.3. Raman and IR studies

A group analytical analysis predicts that there are $19A_1 + 19A_2 + 19B_1 + 19B_2 + 40E$ Brillouin zone center modes for LTB [12]. Among them, the $A_1 + E$ representation describes acoustic modes. The $A_1$ and E modes are IR- and Raman-active, $B_1$ and $B_2$ are Raman-active and $A_2$ modes are silent. For the LNTB structure, the analysis predicts $38A_1 + 38A_2 + 40B_1 + 40B_2$ vibrational modes. The $A_2$ modes are Raman-active and the remaining modes are both Raman-and IR-active. This result indicates that

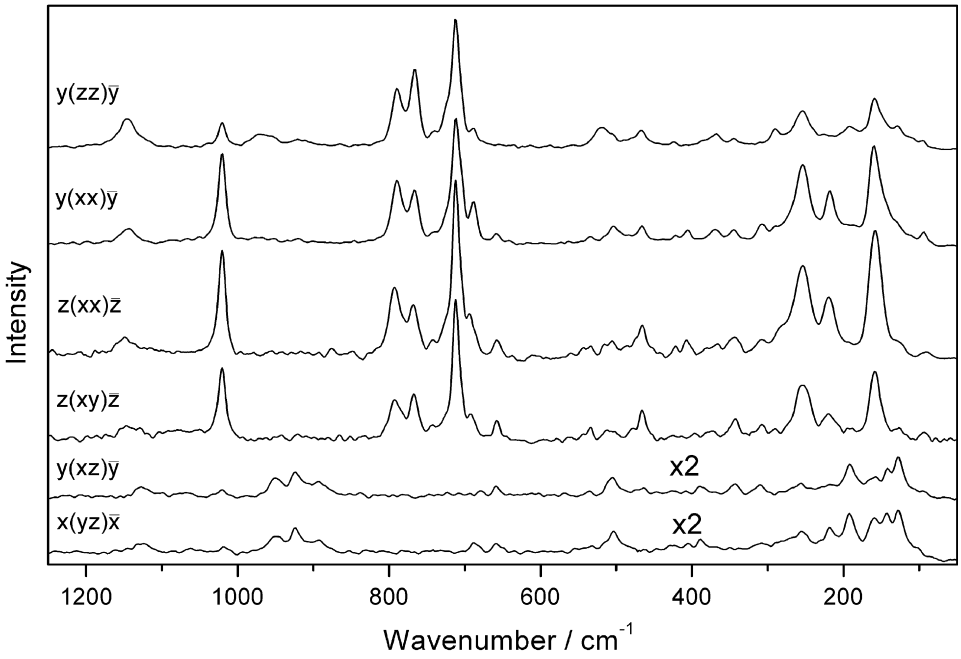


Fig. 5. Polarized Raman spectra of LNTB.

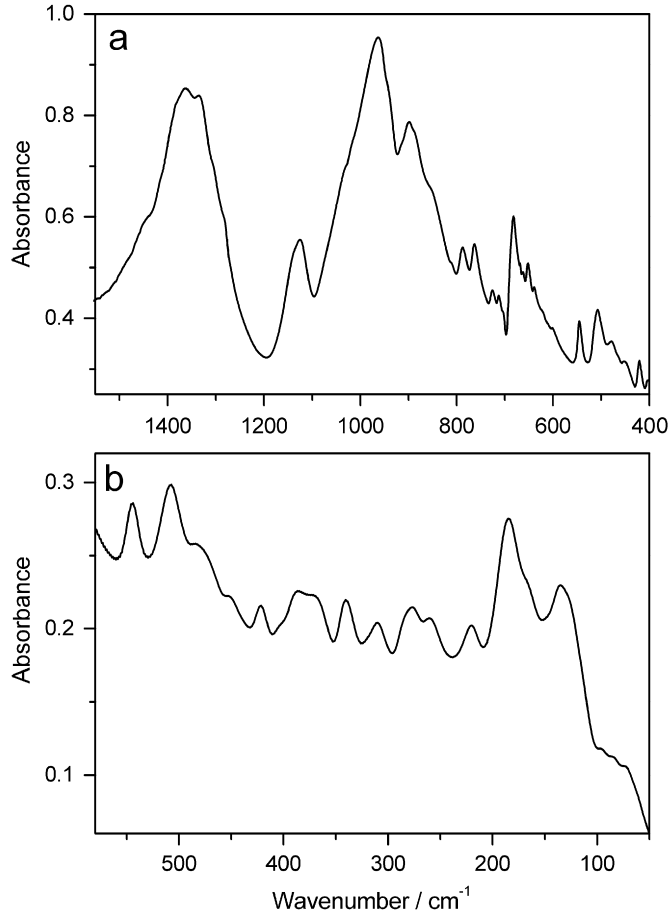


Fig. 6. Polycrystalline IR spectrum of LNTB in the mid-IR (a) and far-IR (b) region.

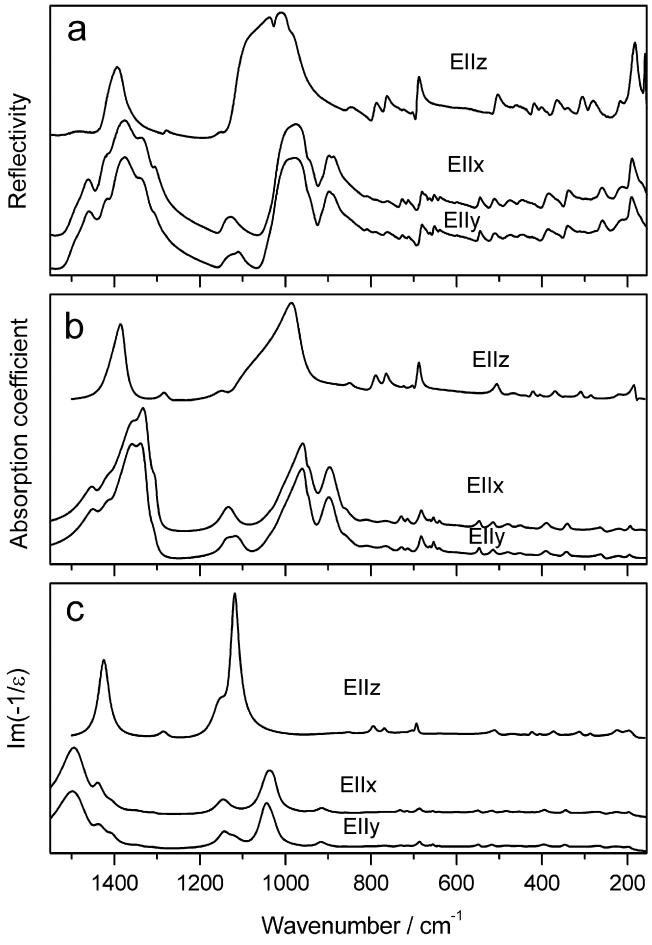


Fig. 7. Infrared reflectivity data for LNTB (a), calculated wavenumber dependence of the absorption coefficient (b) and imaginary part of the inverse dielectric function (c).

symmetry lowering from $I4_1cd$ for LTB to $Fdd2$ for LNTB structure should lead to splitting of the E modes, activation of $A_2$ modes in Raman spectra, as well as activation of the $B_1$ and $B_2$ modes in IR spectra. It should be added that the modes of acoustic branches are $A_1+B_1+B_2$ for LNTB.

The recorded Raman and IR spectra are presented in Figs. 5–7. The IR reflection spectra, shown in Fig. 7, were fitted by using four-parameters model [36] in order to give information about TO and LO wavenumbers. According to this model, the complex dielectric constant is expressed in terms of the IR-active modes as follows:

$$\varepsilon(\omega)=\varepsilon_\infty\prod_j\frac{\omega_{j\mathrm{LO}}^2-\omega^2+\mathrm{i}\omega\gamma_{j\mathrm{LO}}}{\omega_{j\mathrm{TO}}^2-\omega^2+\mathrm{i}\omega\gamma_{j\mathrm{TO}}}, \quad (2)$$

where $\omega_{j\mathrm{TO}}$ and $\omega_{j\mathrm{LO}}$ correspond to the resonance wavenumbers of the $j$th transversal and longitudinal modes, respectively, and $\gamma_{j\mathrm{TO}}$ and $\gamma_{j\mathrm{LO}}$ are the corresponding damping factors. $\varepsilon_\infty$ is the dielectric constant. For normal incidence, the infrared reflectivity $R$ and the dielectric function are related by

$$R=\left|\frac{\sqrt{\varepsilon}-1}{\sqrt{\varepsilon}+1}\right|^2. \quad (3)$$

The results of fitting the experimental data to the four-parameter model are summarized in Table 4, where oscillator strengths $\Delta\varepsilon_{TO}$ are also given.

The observed IR and Raman spectra consist of many bands that should be assigned to respective motions of atoms in the unit cell. Because the structure is made up of $BO_4$ and $BO_3$ groups, which are not independent of each other in the crystal, the assignment of these modes is difficult. Nevertheless, based on similarity between the LTB and LNTB structures, and comparing the measured spectra with those of LTB [12–17] and other borates containing the $BO_4$ ($BiB_3O_6$) [37] and $BO_3$ groups ($K_2Al_2B_2O_7$ [4], $Ca_4GdO(BO_3)_3$ [38], and $Pr_xY_{1-x}Al_3(BO_3)_4$ [39]), we were able to propose assignment of the modes presented in Table 4.

The comparison of the measured spectra, presented in Figs. 5–7, with the literature data for LTB [12–17] shows significant similarities of their phonon properties. Firstly, general contours of the LNTB and LTB spectra are very similar. Moreover, the EII$x$ and EII$y$ spectra, corresponding to the E modes of LTB, look very similar. This behavior indicates that the deviation of the LNTB structure from the tetragonal symmetry is small. Secondly, the Raman spectra show very clear LO–TO splitting for the A modes corresponding to the $A_1$ polar modes of the LTB (see Table 5). The largest splitting (around 6 $cm^{-1}$) is observed for the modes near 790 and 690 $cm^{-1}$. Very similar splitting was observed for the corresponding modes of LTB. It is worth noting, however, that the present IR data show that a number of other modes also exhibit large LO–TO splitting. These are the 975, 1145, and 1380 $cm^{-1}$ $A_1$-symmetry modes which correspond to the $A_1$ polar modes of the LTB, as well as almost all modes observed above 890 $cm^{-1}$ in EII$x$ and EII$y$ polarization, which correspond to the E modes of LTB (see Table 4). The splitting for these modes is not clearly observed in the Raman spectra due to very low intensity of the corresponding modes in Raman scattering.

Although the phonon properties of LNTB and LTB are similar, there are also some important differences. Firstly, many modes of LNTB are shifted towards lower frequency, when compared with the corresponding modes of LTB. This shift does not exceed 10 $cm^{-1}$ for the modes above 500 $cm^{-1}$ and can be attributed to increase in the B–O bond lengths due to presence of larger $Na^+$ ions. Much larger shifts are seen for some modes observed below 500, up to 40 $cm^{-1}$. Since translational modes of alkali metal ions are expected to shift towards the lower frequency when light $Li^+$ ions are substituted by heavier $Na^+$ ions, the observation of the large frequency shifts from some modes in this region can be attributed to significant contribution of alkali metal vibrations in these modes. Secondly, the single $A_1$-symmetry band at 778 $cm^{-1}$ for LTB splits into two bands at 766 and 790 $cm^{-1}$. However, no splitting can be observed for the remaining modes, which correspond to the $A_1$-symmetry modes of LTB. The origin of such a large splitting for this only mode is not known. Thirdly, a few additional bands, not observed for LTB, appear for LNTB due to symmetry lowering. The most characteristic are the Raman bands at 742 and 425 $cm^{-1}$, and the IR bands at 662, 642, 402, and 285 $cm^{-1}$. Fourthly, there are some slight differences in intensities and frequencies of IR bands recorded with light polarized along the $x$-and $y$-axis (see Fig. 6 and Table 4). These spectra should look the same for the tetragonal structure since they correspond to the E modes of LTB. The observed differences can, therefore, be attributed to the lower symmetry of the LNTB crystal.

## 4. Conclusions

We have synthesized the new noncentrosymmetric borate $LiNaB_4O_7$, and we have found that its crystal structure can be regarded as an orthorhombic distortion of the tetragonal parent $Li_2B_4O_7$. An approximate center of symmetry relating the two interpenetrating $(B_4O_7)^3_\infty$ frameworks leads to small SHG tensor components ($d_{jm}\leqslant 0.2$ pm/V). Nevertheless, large single crystals can be grown with $Na_2B_4O_7$ as a flux to compensate for the small nonlinearity, allowing future examination of harmonic conversion to wavelengths below 180 nm with the material.

Distortion from the tetragonal structure of LTB is confirmed from comparison of the Raman and IR spectra for the two materials. The spectra also reveal that LTB and LNTB crystals exhibit very similar LO–TO splitting and oscillator strengths for corresponding modes, further verifying that the two materials have similar electro-optical and nonlinear optical properties.

Table 4
Dispersion parameters for the best fit to the reflectivity data of LNTB for $E||x$, $E||y$, and $E||z$ polarization

| $\omega_{TO}$ ($cm^{-1}$) | $\gamma_{TO}$ ($cm^{-1}$) | $\omega_{LO}$ ($cm^{-1}$) | $\gamma_{LO}$ ($cm^{-1}$) | $\Delta\varepsilon_{TO}$ |
|---|---|---|---|---|
| $E||x$ ($E||y$) | | | | |
| 190.0 (191.0) | 9.4 (11.5) | 195.6 (196.2) | 18.0 (19.8) | 0.454 (0.438) |
| 212.5 (213.2) | 26.3 (30.3) | 216.1 (217.2) | 46.2 (50.6) | 0.161 (0.190) |
| 257.1 (257.3) | 17.6 (14.8) | 257.2 (257.8) | 27.1 (22.1) | 0.011 (0.020) |
| 338.8 (339.7) | 13.2 (17.8) | 339.8 (348.7) | 21.7 (19.9) | 0.293 (0.330) |
| 387.5 (389.6) | 19.7 (20.9) | 392.5 (393.9) | 23.3 (23.5) | 0.113 (0.093) |
| 416.9 (417.3) | 28.5 (36.4) | 417.0 (418.1) | 33.2 (44.0) | 0.001 (0.015) |
| 448.4 (446.7) | 22.2 (22.9) | 450.6 (447.8) | 25.1 (26.4) | 0.051 (0.023) |
| 476.2 (476.7) | 21.9 (22.0) | 478.5 (478.2) | 26.7 (25.0) | 0.046 (0.032) |
| 512.4 (513.6) | 12.9 (14.0) | 514.2 (515.5) | 15.9 (15.3) | 0.034 (0.039) |
| 544.9 (545.8) | 10.5 (8.7) | 546.3 (547.2) | 13.5 (10.1) | 0.025 (0.027) |
| 584.0 (583.3) | 47.8 (51.5) | 584.1 (585.4) | 52.3 (58.1) | 0.021 (0.039) |
| 640.6 (641.8) | 6.3 (7.4) | 640.9 (642.1) | 6.1 (7.0) | 0.008 (0.007) |
| 654.3 (654.2) | 7.7 (8.3) | 655.2 (655.5) | 7.4 (7.3) | 0.019 (0.028) |
| 661.7 (661.7) | 6.7 (7.1) | 662.0 (662.2) | 7.2 (7.5) | 0.004 (0.009) |
| 683.2 (684.2) | 12.6 (13.4) | 685.6 (686.5) | 10.7 (9.2) | 0.052 (0.067) |
| 716.5 (716.0) | 10.3 (14.9) | 717.2 (716.9) | 8.9 (12.8) | 0.014 (0.017) |
| 729.0 (726.8) | 15.5 (17.7) | 731.7 (729.2) | 14.9 (18.7) | 0.046 (0.038) |
| 766.5 (763.0) | 42.5 (32.7) | 769.5 (766.3) | 40.1 (33.5) | 0.053 (0.055) |
| 817.5 (815.1) | 37.9 (40.3) | 818.6 (816.6) | 33.7 (36.3) | 0.023 (0.030) |
| 862.8 (866.3) | 16.5 (21.3) | 862.9 (866.4) | 14.8 (26.1) | 0.001 (0.001) |
| 892.0 (892.3) | 44.3 (46.8) | 916.3 (919.2) | 28.2 (27.8) | 0.614 (0.652) |
| 945.8 (949.2) | 35.1 (31.2) | 949.2 (949.3) | 9.6 (8.5) | 0.150 (0.081) |
| 950.7 (949.8) | 11.0 (9.9) | 1025.2 (1023.1) | 22.8 (24.9) | 0.353 (0.485) |
| 1026.7 (1023.1) | 30.4 (31.1) | 1043.2 (1047.8) | 42.0 (40.0) | 0.003 (0.001) |
| — (1106.4) | — (39.1) | — (1122.1) | — (53.6) | — (0.051) |
| 1129.0 (1138.0) | 40.2 (26.1) | 1146.8 (1142.9) | 40.9 (26.7) | 0.072 (0.009) |
| 1303.0 (1306.9) | 13.6 (18.5) | 1305.3 (1308.5) | 17.2 (19.6) | 0.046 (0.028) |
| 1325.0 (1328.9) | 28.1 (26.6) | 1347.9 (1348.2) | 38.8 (41.3) | 0.295 (0.254) |
| 1356.0 (1357.8) | 35.5 (34.4) | 1407.0 (1405.9) | 25.4 (22.1) | 0.089 (0.106) |
| 1409.4 (1408.9) | 26.0 (24.0) | 1440.9 (1440.2) | 27.9 (35.7) | 0.006 (0.009) |
| 1448.1 (1447.1) | 24.6 (28.0) | 1489.5 (1489.4) | 45.1 (48.8) | 0.009 (0.009) |
| | | $\varepsilon_\infty = 2.81(2.80)$ | | |
| $E||z$ | | | | |
| 182.3 | 7.1 | 191.8 | 25.5 | 0.628 |
| 220.8 | 19.0 | 224.8 | 17.6 | 0.152 |
| 285.0 | 9.8 | 286.7 | 10.5 | 0.064 |
| 307.3 | 10.7 | 310.3 | 14.5 | 0.093 |
| 348.5 | 5.3 | 348.6 | 5.0 | 0.001 |
| 369.3 | 16.0 | 373.1 | 15.3 | 0.107 |
| 406.8 | 8.7 | 407.2 | 7.6 | 0.011 |
| 422.0 | 14.6 | 425.2 | 11.0 | 0.082 |
| 432.4 | 17.8 | 433.0 | 23.0 | 0.011 |
| 465.3 | 27.8 | 468.2 | 29.2 | 0.064 |
| 503.3 | 15.3 | 508.2 | 20.1 | 0.093 |
| 687.5 | 9.8 | 693.2 | 8.5 | 0.053 |
| 700.8 | 7.1 | 700.9 | 9.0 | 0.001 |
| 722.7 | 5.6 | 722.9 | 5.8 | 0.002 |
| 765.7 | 13.3 | 768.5 | 10.6 | 0.041 |
| 790.0 | 17.9 | 794.7 | 14.0 | 0.059 |
| 849.3 | 16.3 | 850.4 | 16.6 | 0.017 |
| 975.3 | 38.7 | 1120.0 | 23.7 | 0.634 |
| 1144.6 | 34.1 | 1153.8 | 42.4 | 0.007 |
| 1281.0 | 21.0 | 1284.0 | 23.0 | 0.009 |
| 1379.7 | 23.2 | 1424.9 | 29.2 | 0.107 |
| | | $\varepsilon_\infty = 2.72$ | | |

Table 5
Raman and IR wavenumbers for LNTB

| Raman | | | | | | IR | | | | Assignment |
|---|---|---|---|---|---|---|---|---|---|---|
| $y(zz)\bar{y}$ $A_1$(TO) | $y(xx)\bar{y}$ $A_1$(TO) | $z(xx)\bar{z}$ $A_1$(LO) | $z(xy)\bar{z}$ $A_2$ | $y(xz)\bar{x}$ $B_1$(TO) | $x(yz)\bar{x}$ $B_2$(TO) | Policrys. | EII$z$ $A_1$(TO) | EII$x$ $B_1$(TO) | EII$y$ $B_2$(TO) | |
| — | — | — | — | — | — | 1446*sh* | — | 1448*w* | 1447*w* | $\nu_3(BO_3)$ |
| — | — | — | — | — | — | — | — | 1409*w* | 1409*w* | |
| — | — | — | — | — | — | — | 1380*s* | — | — | |
| — | — | — | — | — | — | 1363*s* | — | 1356*m* | 1358*m* | |
| — | — | — | — | — | — | 1334*m* | — | 1325*s* | 1329*s* | |
| — | — | — | — | — | — | — | — | 1303*w* | 1307*w* | |
| — | — | — | — | — | — | 1280*sh* | 1281*w* | — | — | |
| 1146*m* | 1145*w* | 1148*w* | 1147*vw* | — | — | 1143*sh* | 1145*w* | — | — | $\nu_1(BO_3)+$ |
| — | — | — | — | 1127*w* | 1126*w* | 1125*m* | — | 1129*m* | 1138*w* | $\nu_3(BO_4)$ |
| — | — | — | — | — | — | — | — | — | 1106*m* | |
| — | — | — | — | 1068*vw* | 1062*vw* | — | — | — | — | |
| 1021*w* | 1021*s* | 1021*m* | 1021*m* | 1021*vw* | 1020*vw* | 1031*sh* | | 1027*w* | 1023*w* | |
| 968*w* | — | — | — | — | — | — | 975*s* | — | — | |
| — | — | — | — | 951*w* | 950*w* | 963*s* | — | 951*S* | 950*s* | |
| — | — | — | — | — | — | — | — | 946*m* | 949*w* | |
| — | — | — | — | 923*w* | 923*vw* | — | — | — | — | |
| — | — | — | — | 894*w* | 893*vw* | 899*m* | — | 892*s* | 892*s* | |
| — | — | — | — | — | — | — | — | 863*vw* | 866*w* | |
| — | — | — | — | — | — | 855*sh* | 849*w* | — | — | |
| — | — | — | — | — | — | 810*vw* | — | 817*w* | 815*w* | |
| 789*m* | 789*m* | 795*m* | 794*m* | — | — | 787*w* | 790*m* | — | — | $\nu_4(BO_3)$ |
| 766*m* | 766*m* | 769*m* | 767*m* | — | — | 763*vw* | 766*m* | 766*w* | 763*w* | |
| 741*w* | 742*w* | 742*w* | 742*w* | — | — | — | — | — | — | |
| 724*sh* | 724*sh* | 724*sh* | 724*sh* | — | — | 726*w* | 723*vw* | 729*w* | 727*w* | |
| 712*s* | 712*s* | 712*s* | 712*s* | — | — | 713*w* | 701*vw* | 717*w* | 716*w* | |
| 689*w* | 688*w* | 694*w* | 694*w* | 683*w* | 688*w* | — | 687*m* | — | — | $\nu_2(BO_3)$ |
| — | — | — | — | — | — | 682*m* | — | 683*m* | 684*m* | |
| — | 658*w* | 658*w* | 658*w* | 659*vw* | 659*w* | 662*vw* | — | 662*vw* | 662*vw* | |
| — | — | — | — | — | — | 652*w* | — | 654*w* | 654*w* | |
| — | — | 607*w* | — | — | — | 639*vw* | — | 641*vw* | 642*vw* | |
| — | — | — | — | — | — | — | — | 584*w* | 583*w* | |
| — | — | 543*w* | 543*vw* | 536*vw* | — | 545*w* | — | 545*w* | 546*w* | $\nu_1(BO_4)+$ |
| — | 535*w* | 533*vw* | 534*vw* | — | — | — | — | — | — | $T'(Li^+)$ |
| 518*w* | — | 515*vw* | 512*w* | — | — | 506*w* | 503*w* | — | — | $+T'(BO_3)$ |
| — | 503*w* | 507*w* | 507*w* | 504*w* | 503*w* | — | — | 512*w* | 514*w* | |
| — | — | — | — | — | — | 478*m* | — | 476*w* | 477*w* | |
| 467*w* | 466*w* | 466*m* | 466*w* | 464*vw* | — | — | 465*w* | — | — | |
| — | — | — | — | — | — | 451*w* | — | 448*w* | 447*w* | |
| | — | — | — | — | — | — | 432*vw* | — | — | |
| 424*vw* | 422*vw* | 422*w* | 425*w* | — | 428*vw* | 420*vw* | 422*w* | 417*w* | 417*w* | $\nu_4(BO_4)+$ |
| — | 406*w* | 407*vw* | — | — | 406*vw* | — | 402*vw* | — | — | $\nu_2(BO_4)+$ |
| — | — | — | 397*vw* | 390*w* | 389*w* | 386*w* | — | 388*w* | 390*w* | $L(BO_3)+$ |
| 368*w* | 370*w* | 366*w* | 374*w* | — | — | 372*vw* | 369*w* | — | — | $T'(Na^+)$ |
| 345*w* | 345*w* | 345*w* | 345*w* | 343*w* | — | 340*w* | 348*vw* | 339*w* | 340*w* | |
| — | 307*w* | 308*vw* | 308*w* | 310*w* | 308*vw* | 311*w* | 307*w* | — | — | |
| 291*w* | — | — | 291*vw* | — | — | 277*w* | 285*w* | — | — | |
| 254*m* | 254*m* | 254*m* | 254*m* | 256*w* | 256*w* | 260*w* | — | 257*w* | 257*w* | |
| — | 217*m* | 219*w* | 219*w* | — | 217*w* | 220*w* | 221*w* | 213*w* | 213*w* | |
| 192*w* | — | — | 188*vw* | 192*w* | 1922 | 185*m* | 182*w* | 190*w* | 191*w* | |
| 159*m* | 159s | 158*m* | 158*m* | 158*w* | 160*w* | — | — | — | — | |
| — | — | — | — | 142*w* | 142*w* | — | — | — | — | |
| 129*vw* | — | — | 127*vw* | 129*w* | 129 | 135 | — | — | — | |
| — | 94*w* | 94*w* | 94*w* | — | — | 95*vw* | — | — | — | |

The modes observed in polarization $y(zz)-y$, $y(xx)-y$, $z(xx)-z$, $z(xy)-z$, and $y(xz)-y$ (or $x(yz)-x$) correspond to $A_1$(TO), $A_1$(TO) + $B_2$, $A_1$(LO) + $B_2$, $B_1$(TO), and E(TO + LO) modes of $Li_2B_4O_7$, respectively.

## References

[1] A.A. Kaminskii, P. Becker, L. Bohaty, S.N. Bagaev, H.J. Eichler, K. Ueda, J. Hanuza, H. Rhee, H. Yoneda, K. Takaichi, I. Terashima, M. Maczka, Laser Phys. 13 (2003) 1385.

[2] G. Aka, A. Kahn-Harari, F. Mougel, D. Vivien, F. Salin, P. Coquelin, P. Colin, D. Pelenc, J.P. Damelet, J. Opt. Soc. Am. B 14 (1997) 2238.

[3] J.F.H. Nicholls, B. Henderson, B.H.T. Chai, Opt. Mater. 16 (2001) 453.

[4] X.B. Hu, J.Y. Wang, C.Q. Zhang, X.G. Xu, C.K. Loong, M. Grimsditch, Appl. Phys. Lett. 85 (2004) 2241.
[5] R. Komatsu, T. Sugawara, K. Sassa, N. Sarukura, Z. Liu, S. Izumida, Y. Segawa, S. Uda, T. Fukuda, K. Yamanouchi, Appl. Phys. Lett. 70 (1997) 3492.
[6] U. Chatterjee, S. Gangopadhyay, C. Ghosh, G.C. Bhar, Appl. Opt. 44 (2005) 817.
[7] B. Wu, F. Xie, C.C.D. Deng, Z. Xu, Opt. Commun. 88 (1992) 451.
[8] A.S. Bhalla, L.E. Cross, R.W. Whatmore, Jpn. J. Appl. Phys. 24 (1985) 727.
[9] C. Furetta, P.S. Weng, Operation Thermoluminescent Dosimetry, World Scientific, London, 1998.
[10] J. Krogh-Moe, Acta Crystallogr. B 24 (1968) 179.
[11] M. Natarajan, R. Faggiani, I.D. Brown, Cryst. Struct. Commun. 8 (1979) 367.
[12] G.L. Paul, W. Taylor, J. Phys. C 15 (1982) 1753.
[13] N.D. Zhigadlo, M. Zhang, E.K.H. Salje, J. Phys.: Condens. Matter 13 (2001) 6551.
[14] A.V. Vdovin, V.N. Moiseenko, V.S. Gorelik, Ya. Burak, Phys. Sol. State 43 (2001) 1648.
[15] Y. Li, G. Lan, J. Phys. Chem. Solids 57 (1996) 1887.
[16] S.I. Furusawa, S. Tange, Y. Ishibashi, K. Miwa, J. Phys. Soc. Japan 59 (1990) 1825.
[17] A. Elbelrhiti Elalaoui, A. Maillard, M.D. Fontana, J. Phys.: Condens. Matter 17 (2005) 7441.
[18] A. Majchrowski, M.T. Borowiec, E. Michalski, J. Cryst. Growth 264 (2004) 201.
[19] Oxford Diffraction, CrysAlis CCD Version 1.171.30.3, Oxford Diffraction, Ltd., Oxford, UK, 2004.
[20] Oxford Diffraction, CrysAlis RED Version 1.171.30.3, Oxford Diffraction, Ltd., Oxford, UK, 2004.
[21] G.M. Sheldrick, SHELXS97, Program for Solution of the Crystal Structures, University of Göttingen, 1997.
[22] G.M. Sheldrick, SHELXL99, Program for Crystal Structure Refinement, University of Göttingen, 1997.
[23] S.W. Kurtz, T.T. Perry, J. Appl. Phys. 39 (1968) 398.
[24] K.I. Schaffers, Ph.D. Dissertation, Oregon State University, 1993.
[25] G.A. Peterson, Ph.D. Disseration, Oregon State University, 1997.
[26] P. Becker, J. Liebertz, L. Bohaty, J. Cryst. Growth 203 (1999) 149.
[27] S.F. Radaev, B.A. Maximov, V.I. Simonov, Acta Crystallogr. B 48 (1992) 154.
[28] J. Krogh-Moe, Acta Crystallogr. B 30 (1974) 578.
[29] J. Krogh-Moe, Acta Crystallogr. B 28 (1972) 3089.
[30] Y. Ono, M. Nakaya, T. Kajitani, T. Sugawara, M. Watanabe, H. Shiraishi, R. Komatsu, Acta Crystallogr. C 56 (2000) 1413.
[31] I.D. Brown, D. Altermatt, Acta Crystallogr. B 41 (1985) 240.
[32] I.D. Brown, Acta Crystallogr. B 48 (1992) 553.
[33] T. Sugawara, R. Komatsu, S. Uda, Solid State Commun. 107 (1998) 233.
[34] Y.X. Fan, R. Schlecht, M.W. Qiu, D. Luo, A.D. Jiang, Y.C. Huang, in: L.L. Chase, A.A. Pinto (Eds.), OSA Proceedings on Advanced Solid-State Lasers, 13, 1992, p. 371.
[35] R. Komatsu, T. Sugawara, N. Watanabe, S. Uda, V. Petrov, Rev. Laser Eng. 27 (1999) 541.
[36] F. Gervais, P. Echegut, in: R. Blinc, A.P. Levanyuk (Eds.), Incommensurate Phases in Dielectrics, North Holland, Amsterdam, 1986, p. 337.
[37] X. Hu, J. Wang, B. Teng, C.-K. Loong, M. Grimsditch, J. Appl. Phys. 97 (2005) 33501.
[38] M. Maczka, J. Hanuza, A. Pajączkowska, Y. Morioka, J.H. Van der Maas, J. Raman, Spectroscopy 35 (2004) 266.
[39] H.R. Xia, L.X. Li, J.Y. Wang, W.T. Yu, P. Yang, J. Raman, Spectroscopy 30 (1999) 557.